



Smith, E. C., Baird, A., Kendall, J. M., Martin, C., White, R. S., Brisbourne, A. M., & Smith, A. M. (2017). Ice fabric in an Antarctic ice stream interpreted from seismic anisotropy. *Geophysical Research Letters*, 44(8), 3710–3718. DOI: 10.1002/2016GL072093

Peer reviewed version

Link to published version (if available):
[10.1002/2016GL072093](https://doi.org/10.1002/2016GL072093)

[Link to publication record in Explore Bristol Research](#)
PDF-document

This is the author accepted manuscript (AAM). The final published version (version of record) is available online via [insert publisher name] at [insert hyperlink]. Please refer to any applicable terms of use of the publisher.

University of Bristol - Explore Bristol Research

General rights

This document is made available in accordance with publisher policies. Please cite only the published version using the reference above. Full terms of use are available:
<http://www.bristol.ac.uk/pure/about/ebr-terms.html>

Abstract

Here we present new measurements of an anisotropic ice fabric in a fast moving (377 ma^{-1}) ice stream in West Antarctica. We use ~ 6000 measurements of shear wave splitting observed in microseismic signals from the bed of Rutford Ice Stream, to show that in contrast to large-scale ice flow models, which assume that ice is isotropic, the ice in Rutford Ice Stream is dominated by a previously unobserved type of partial girdle fabric. This fabric has a strong directional contrast in mechanical properties, shearing 9.1 times more easily along the ice flow direction than across flow. This observed fabric is likely to be widespread and representative of fabrics in other ice streams and large glaciers, suggesting it is essential to consider anisotropy in data-driven models to correctly predict ice loss and future flow in these regions. We show how passive microseismic monitoring can be effectively used to provide these data.

1 Introduction

As ice flows, its internal structure changes in response to the stresses it has encountered. Understanding the types of structure, known as ice fabrics, formed in different flow environments is needed for accurate prediction of the future behaviour of ice sheets using ice flow models [Azuma, 1994]. Glacial ice is formed of hexagonal ice crystals, known as Ih ice [Faria *et al.*, 2014a]. These crystals are strongly anisotropic, the viscosity is around 60 times less along the basal plane (normal to the *c*-axis) than perpendicular to it [Duval *et al.*, 1983], meaning the ice is softer and deforms preferentially on this plane by slip (ice creep). This causes *c*-axes in a bulk polycrystalline ice mass to rotate when under stress, forming a preferred crystal orientation fabric (COF) which is also anisotropic. The type of COF formed records the deformation history of ice and the viscosity of the COF will affect future ice flow [Alley, 1988]. *In situ* measurements of ice COF are most commonly made over slow moving ice at ridges and domes (e.g. Faria *et al.* [2014a,b]; Matsuoka *et al.* [2012]) with very few measurements made in fast moving ice stream environments. Ice streams are the key discharge pathways of the Greenland and Antarctic ice sheets. Lack of observational data in these key regions limits our ability to model their flow and evolution [Gagliardini *et al.*, 2009] and thus the future of the ice sheets themselves and their contribution to global sea level. Here we present measurements of a strong ice fabric in Rutford Ice Stream, Antarctica. We measure seismic shear wave anisotropy observed in icequake signals generated at the base of Rutford Ice Stream to assess the ice fabric properties in this region.

2 Site Location and Observed Shear Wave Splitting

In Rutford Ice Stream, Antarctica, 40 km upstream of the grounding line, the ice flows at an average velocity of 377 ma^{-1} [Murray *et al.*, 2007]. In this area the ice is around 2.2 km thick and 25 km wide (Fig. 1a) and has been flowing in a laterally-confined ice stream environment for around 150 km. As the ice flows, seismicity is generated by basal sliding over ‘sticky spots’ at the base of the ice stream [Smith, 2006; Smith *et al.*, 2015]. Seismic energy radiates outwards from the source as elastic body waves, longitudinal P-waves and transverse S-waves (shear waves), which are detected by three-component receivers at the ice surface (Fig. 1b). A clear indication that these elastic waves have travelled through an anisotropic ice fabric is the presence of two independent S-waves (S1 and S2, Fig. 1b). When an S-wave, generated at the base of the ice stream, encounters a region of anisotropic ice it will split into two orthogonal S-waves, this is known as shear wave splitting (SWS) or seismic birefringence. The two split S-waves propagate independently, arriving at a receiver separated by a delay time and with directions of polarisation controlled by the anisotropic symmetry axis of the fabric they have traveled through [Savage, 1999]. We measure this delay time (δt), which is proportional to the strength of

anisotropy, and the polarisation direction of the fastest S-wave (Φ), which is an indicator of the anisotropic symmetry of the medium.

The data set used in this study contains ~ 3000 basal seismic events with high signal to noise ratio S-waves, recorded at 10 receivers [Smith *et al.*, 2015]. This means there are $\sim 30,000$ shear wave splitting measurements to be made, one for each pair of shear wave arrivals on each station for each event. We use the automated approach of *Wuestefeld et al.* [2010] to make these measurements, which provides an effective method of processing a large quantity of data. Ray paths from each event to each station cover a variety of azimuths and inclinations, which allows us to effectively sample the ice fabric in this area and derive the elastic anisotropy. From the elastic anisotropy we then infer the *in situ* anisotropic ice COF.

3 Shear Wave Splitting Analysis and Results

The automated method of *Wuestefeld et al.* [2010] determines the combination of polarisation direction of the fastest S-wave (Φ) and delay time (δt) which best remove the effects of shear-wave splitting for each of the $\sim 30,000$ pairs of shear waves in this dataset. The method also calculates an automated quality factor (Q) of the resulting shear wave splitting measurements which can then be used to filter the results by determining a threshold of Q above which the measurements are of a suitable quality. Before the data were processed the seismic waveforms for each event were rotated into geographical: East, North, Vertical (ENZ) orientation from the field orientation of XYZ. Waveforms were not rotated into the ray frame before analysis, as is commonly the case for SWS analysis. Arrivals in this data set are near vertical, due to refraction caused by a low velocity firm layer at the surface (~ 100 m in thickness). This means the majority of the S-wave energy is recorded on the horizontal components (E and N), which will be used in the SWS analysis, and therefore rotation is not necessary.

The method of *Wuestefeld et al.* [2010] can be summarised as follows: An analysis time window is defined around the picked S-wave arrivals on the horizontal (E and N) components of a station. Within this window a robust grid search is performed over all possible values of polarisation directions ($-90^\circ < \Phi < 90^\circ$) and delay time ($0 < \delta t < 0.1$ s). As the analysis is very sensitive to the length of the analysis time window [Teauby *et al.*, 2004], the analysis is repeated for a range of window lengths. The values of Φ and δt which are most stable over this range of window lengths is assessed using the cluster analysis method of *Teauby et al.* [2004]. The combination of parameters that provides the best removal of splitting is assessed using two different methods. The first, the XC method, is based on cross-correlating the corrected S-wave waveforms to assess similarity. The second, the EV method, is based on assessing the extent to which particle motion of the corrected waveforms has been linearised, using the method of *Silver and Chan* [1991]. A comparison between the values of the splitting parameters, Φ and δt , determined using the two methods allows the automated identification of good results by calculating a quality factor (Q), where $Q = 1$ indicates a good splitting measurement. By manual inspection of a sub-set of the results, splitting measurements with a signal-to-noise ratio > 7.5 and $Q > 0.8$ were selected yielding a total of 5951 shear wave splitting measurements.

The strength of the anisotropy along a ray path can be expressed as a percentage difference in velocity between the fast and slow waves using

$$\delta V_s = (\overline{V_s} \times \delta t \times 100) / r, \quad (1)$$

where $\overline{V_s} = 1944 \text{ ms}^{-1}$, is the average isotropic S-wave velocity and r is the source-receiver straight line distance for a given measurement (details on event location given in *Smith et al.* [2015]). It should be noted, that while the arrivals are refracted in the near-surface firm layer, the majority of the travel-path of a given shear-wave is in the ice column. This means a source-receiver straight line distance is a reasonable approximation for the true

122 travel path (differences at maximum offset are around 10-20 m, which is within the loca-
123 tion error - details in *Smith et al. [2015]*).

124 The resulting values plotted on an upper hemisphere projection (Fig. 2) show that
125 SWS measurements cover a wide range of ray path azimuths, and inclinations out to 73°.
126 The measurements show that the dominant polarisation direction of the fast S-wave (Φ) is
127 perpendicular to the ice flow direction and the strongest seismic anisotropy (δV_s) occurs
128 in the near vertical ray paths. There is no systematic variation in Φ for different regions
129 of the ice stream suggesting the ice fabric in this area is uniform and all measurements
130 can be treated as sampling the same fabric at a variety of ray azimuths and inclinations.
131 The measurements show a clear trend of greatest δV_s in the vertical (centre of the plot),
132 weakening with increasing inclination angle (edge of the plot). There are also azimuthal
133 variations in δV_s and Φ , which are especially evident for ray paths with inclinations of
134 30° to 60°.

143 4 Modeling for Ice COF

144 In order to determine the type of ice fabric that would cause this pattern of shear-
145 wave splitting we use a forward model of elastic wave propagation through anisotropic
146 ice fabrics to calculate the theoretical SWS for a given ice fabric type. Elasticity tensors
147 derived from *Maurel et al. [2015]* are used to determine the phase velocities, and thus the
148 modelled shear wave splitting parameters (δV_{sM} and Φ_M) associated with S-waves travel-
149 ling through the specified fabric at different azimuths and inclinations.

150 To define the misfit between measured and modeled splitting parameters, we first
151 express them as vectors (with lengths δV_s and δV_{sM} , and orientations Φ and Φ_M respec-
152 tively). The two are then subtracted to find the residual vector. The global misfit, f , to be
153 minimised in our inversion is simply the summation of the magnitude of the residuals for
154 all n of the SWS measurements:

$$f = \sum_n \sqrt{(\delta V_s \sin 2\Phi - \delta V_{sM} \sin 2\Phi_M)^2 + (\delta V_s \cos 2\Phi - \delta V_{sM} \cos 2\Phi_M)^2}, \quad (2)$$

155 the factor of 2 in the trigonometric functions in (2) accounts for the fact that Φ has 180°
156 periodicity rather than 360°. It should be noted that prior to this process, measured SWS
157 values are averaged within inclination and azimuth bins of 5° × 5° in order to avoid a sys-
158 tematic bias in the model fit to regions where there are a higher density of measurements.

159 Fabrics commonly observed elsewhere in ice, transversely isotropic with either ver-
160 tical or horizontal axes of symmetry (VTI, HTI), can be eliminated as the sole cause of
161 anisotropy in this survey area [*Harland et al., 2013*] for the following reasons: pure VTI
162 (cluster fabric) would show a minimum δV_s for vertically-propagating waves, and pure
163 HTI (thick girdle) would show high δV_s across all inclinations perpendicular to the ice
164 flow direction (Fig. 3), neither of which match the observations (Fig. 2). Therefore, three
165 polycrystalline ice fabric models were tested, combining a cluster fabric with varying de-
166 grees of three different girdle fabrics (Fig. 3): a thick girdle, a vertical partial girdle (par-
167 tial girdle of *Maurel et al. [2015]*) and a horizontal partial girdle fabric (vertical partial
168 girdle rotated 90° in the X_2 plane). The elasticity tensors describing these mixed fabric
169 models are calculated using a Voigt-Reuss-Hill average [*Hill, 1952*]. For each of the three
170 starting models, the misfit (Equation 2) is calculated for all variable parameters (opening
171 angles and proportions of each input fabric) to indicate the fabric model which best fits
172 the data.

173 The ice fabric model that provides the best fit to the observed SWS measurements
174 is comprised of a mixture of 47% horizontal partial girdle (HPG), an orthorhombic fabric
175 with a narrow opening angle of $\theta = 22^\circ$, orientated near orthogonal to the ice flow direc-
176 tion (Fig. 4a) and 53% cluster fabric with an opening angle of $\theta = 73^\circ$ (Fig. 4b). While
177 partial girdle fabrics have been commonly hypothesised in the literature (e.g. *Nanthikesan*

178 and Shyam Sunder [1994]; Maurel et al. [2015]; Diez and Eisen [2015]) the HPG ice fab-
 179 ric has not been observed in glacial ice before; henceforth we refer to the mixed HPG and
 180 cluster fabric as ‘diffuse HPG’.

200 5 Discussion

201 The fit between modeled SWS results using the diffuse HPG fabric model and the
 202 observed SWS measurements is very good (Fig. 4c) with an average misfit per measure-
 203 ment of only $\sim 1.2\%$. Both the orientation of the fast S-wave and the pattern in strength of
 204 splitting match well. The azimuthal variation in the pattern of splitting is recreated well
 205 by the ice fabric model, for example the lobes of alternating high and low δV_s between
 206 30° and 60° ray path inclination. There are relatively few measurements where lobes of
 207 high δV_s are modeled at 50° and 230° azimuth at high inclinations; these are the only ar-
 208 eas where the model cannot be tested. In the diffuse HPG fabric the pattern of S-wave
 209 anisotropy is largely influenced by the HPG component, as can be seen by comparing Fig.
 210 4a and Fig. 4c. The cluster component of diffuse HPG (Fig. 4b) is broad and as a fabric
 211 it has a low degree of anisotropy, verging on isotropic, which serves to reduce the over-
 212 all strength of the final mixed fabric without having a strong influence on the pattern of
 213 SWS.

214 The formation of an HPG ice fabric is consistent with a stress regime of lateral
 215 compression across-flow and longitudinal extension along the ice flow direction. As ice
 216 undergoes viscous deformation the c-axes of the crystals rotate towards the axis of great-
 217 est compressive strain and away from the axis of extension [Alley, 1992]. Minchew et al.
 218 [2016] use satellite interferometry to extract the detailed surface strain-rate of Rutford Ice
 219 Stream. Their observations show that in our area of study there are along-flow positive de-
 220 viatoric normal strain rates (extension) combined with significant across-flow negative de-
 221 viatoric normal strain rates (compression). Ice flow with no lateral compression and pure
 222 longitudinal extension would form a thick girdle perpendicular to the ice flow direction.
 223 The addition of significant lateral compression causes c-axes to rotate towards the axis of
 224 compression, in the horizontal plane and across the flow, promoting the formation of HPG
 225 fabric. The stronger the lateral compression is in relation to the along-flow extension, the
 226 smaller the opening angle of the HPG (θ , Fig. 4a). The origin of the broad cluster fabric
 227 is less intuitive in this environment; it could be a remnant fabric from a previous stress
 228 regime that has not been completely modified; or a modification of the flow-induced HPG
 229 fabric by dynamic recrystallisation and polygonisation [Gagliardini et al., 2009]. The split-
 230 ting measurements are not frequency dependant (measurements are the same on data fil-
 231 tered to different bandwidths) and there is no clear ‘double split’ (when the shear waves
 232 are split twice by travelling through layers with different anisotropic properties) in these
 233 data. This suggests there are not two discrete layers, one of a cluster fabric and one of
 234 an HPG fabric and that the model can be well represented by a homogeneous anisotropic
 235 diffuse HPG medium.

236 As shown experimentally [Pimienta et al., 1987], a macroscopic sample of ice with
 237 all the c-axes of its crystals orientated in the same direction deforms ten times faster than
 238 an equivalent isotropic sample, when it is sheared parallel to the basal planes. We deter-
 239 mine the effect of the measured fabric on the mechanical properties of ice by considering
 240 it as a polycrystalline sample of ice containing 47% of the crystals in a pure HPG fabric
 241 and the rest isotropic (a reasonable approximation to a broad cluster), and assuming the
 242 uniform stress approximation of Lliboutry [1993]. Such a fabric results in ice which is 9.1
 243 times easier to shear along the flow direction than horizontally across the flow direction.

244 Large-scale ice flow models (e.g. Favier et al. [2014]; Deconto and Pollard [2016];
 245 Gillet-Chaulet et al. [2016]) assume that ice is isotropic. There are a number of justifica-
 246 tions for this, other than our lack of knowledge about fabric or the numerical difficulty in
 247 incorporating anisotropy. A key justification is that the majority of *in situ* ice COF mea-

248 surements are made at ice domes or ridges. Ice COF in these areas is formed by hori-
 249 zontal shear and vertical compression, promoting the formation of cluster COF fabrics
 250 (Fig. 3a). Cluster fabrics are not rheologically anisotropic in the horizontal and there-
 251 fore the overall effect of such an ice fabric can be simulated with a local change in vis-
 252 cosity, known as an enhancement factor [Ma *et al.*, 2010]. However, our observations
 253 of fabric in a fast flowing ice stream show a strong contrast in mechanical properties of
 254 the ice along and across the flow direction. The use of enhancement factors to assimilate
 255 ice viscosity changes is also justified when a flow regime does not change significantly
 256 over the time of a model simulation. Models tend to be initialised with known surface ice
 257 flow velocity data. Therefore, in a situation where ice flow conditions are stable over a
 258 model simulation, and thus the strain conditions are stable over this period, the final strain
 259 regime should be equivalent to the initialised one. However, we have evidence of recent
 260 changes in the direction of large Antarctic ice streams due to deglaciation (e.g., Conway
 261 *et al.* [2002]; Bingham *et al.* [2015]), leading to a possible misalignment between the flow-
 262 induced fabric and the present-day flow direction. In these cases the use of an enhance-
 263 ment factors is no longer a valid representation of ice viscosity. The mechanical properties
 264 of an ice fabric will also play an important role in ice fracture, for example during calv-
 265 ing, which is an essential mechanism for rapid ice loss in Antarctica [Pollard *et al.*, 2015].

266 Ice streams, such as Rutford Ice Stream, which are characterised by initial conver-
 267 gent ice flow followed by lateral confinement along much of their length [Minchew *et al.*,
 268 2016], are seen across much of Antarctica [Ng, 2015] and Greenland [Bons *et al.*, 2016].
 269 It is therefore likely that the diffuse HPG fabric found here will be present in other fast-
 270 flowing ice stream environments. Ice streams are the key pathways of ice discharge from
 271 Antarctica and Greenland and therefore understanding how strain-induced ice fabric modi-
 272 fies the flow of ice in these regions is essential.

273 6 Conclusions

274 This is the first conclusive study of which we are aware that provides a robust model
 275 of ice stream fabric using shear wave splitting in microseismic data. A study on the down-
 276 stream ice plain of Whillans Ice Stream [Picotti *et al.*, 2015] found that a weakly anisotropic
 277 cluster fabric dominated the entire ice depth and suggested that this may be typical of
 278 “large ice streams in regions where basal sliding and bed deformation dominate over in-
 279 ternal glacial deformation”. Here we provide clear evidence that this is not the case in
 280 Rutford Ice Stream, West Antarctica, which is also a large Antarctic ice stream moving
 281 primarily by basal sliding and sediment deformation [Smith and Murray, 2009]. Many of
 282 the commonly investigated ice fabrics in the literature thus far have been based upon those
 283 seen in ice cores, drilled at the interior of ice sheets. We have observed an additional cat-
 284 egory of ice fabric, the horizontal partial girdle, formed by strong horizontal confinement
 285 with longitudinal extension. In this study, we have provided new evidence of ice fabric
 286 structure in ice stream environments and shown that microseismic monitoring is an effec-
 287 tive tool for investigating this. Neglecting such an ice fabric could lead to errors in mod-
 288 eled projections of ice flow, and thus reduce our ability to estimate the future contribution
 289 of ice sheets to sea level.

290 Acknowledgments

291 E.C.S. was funded by a Natural Environment Research Council (NERC) PhD Studentship
 292 through the British Antarctic Survey (BAS). The work was supported by the UK Natu-
 293 ral Environment Research Council under grant NE/B502287/1; equipment was provided
 294 by NERC Geophysical Equipment Facility (loan 852). We thank BAS Operations, H.D.
 295 Pritchard and C. Griffiths for data collection. Data are available through NERC’s Polar
 296 Data Centre (<http://pdc.nerc.ac.uk/>). Department of Earth Sciences, University of Cam-
 297 bridge contribution number ESCXXXX.

298 **References**

- 299 Alley, R. (1992), Flow-law hypotheses for ice-sheet modeling, *J. Glaciol.*, *38*, 245–256.
- 300 Alley, R. B. (1988), Fabrics in polar ice sheets: development and prediction, *Science*, *240*,
- 301 493–495, doi:10.1126/science.240.4851.493.
- 302 Azuma, N. (1994), A flow law for anisotropic ice and its application to ice sheets, *Earth*
- 303 *Planet. Sci. Lett.*, *128*, 601–614, doi:10.1016/0012-821X(94)90173-2.
- 304 Bingham, R. G., D. M. Rippin, N. B. Karlsson, H. F. J. Corr, F. Ferraccioli, T. a. Jor-
- 305 dan, A. M. Le Brocq, K. C. Rose, N. Ross, and M. J. Siegert (2015), Ice-flow struc-
- 306 ture and ice dynamic changes in the Weddell Sea sector of West Antarctica from
- 307 radar-imaged internal layering, *J. Geophys. Res. Earth Surf.*, *120*, 655–670, doi:
- 308 10.1002/2014JF003291.
- 309 Bons, P. D., D. Jansen, F. Mundel, C. C. Bauer, T. Binder, O. Eisen, M. W. Jessell, M.-
- 310 G. Llorens, F. Steinbach, D. Steinhage, and I. Weikusat (2016), Converging flow and
- 311 anisotropy cause large-scale folding in Greenland’s ice sheet., *Nat. Commun.*, *7*, 11,427,
- 312 doi:10.1038/ncomms11427.
- 313 Conway, H., G. Catania, C. Raymond, A. Gades, T. A. Scambos, and H. Engelhardt
- 314 (2002), Switch of flow direction in an Antarctic ice stream, *Nature*, *419*, 456–467, doi:
- 315 10.1038/nature01081.
- 316 Deconto, R. M., and D. Pollard (2016), Contribution of Antarctica to past and future sea-
- 317 level rise, *Nature*, *531*(7596), 591–597, doi:10.1038/nature17145.
- 318 Diez, A., and O. Eisen (2015), Seismic wave propagation in anisotropic ice - Part 1: Elas-
- 319 ticity tensor and derived quantities from ice-core properties, *The Cryosphere*, *9*, 367–
- 320 384, doi:10.5194/tc-9-367-2015.
- 321 Duval, P., M. F. Ashby, and I. Andermant (1983), Rate-Controlling Processes in the Creep
- 322 of Polycrystalline Ice, *J. Phys. Chem.*, *87*, 4066–4074, doi:10.1021/j100244a014.
- 323 Faria, S. H., I. Weikusat, and N. Azuma (2014a), The microstructure of polar ice. Part II:
- 324 State of the art, *J. Struct. Geol.*, *61*, 21–49, doi:10.1016/j.jsg.2013.11.003.
- 325 Faria, S. H., I. Weikusat, and N. Azuma (2014b), The microstructure of polar
- 326 ice. Part I: Highlights from ice core research, *J. Struct. Geol.*, *61*, 2–20, doi:
- 327 10.1016/j.jsg.2013.09.010.
- 328 Favier, L., G. Durand, S. L. Cornford, G. H. Gudmundsson, O. Gagliardini, F. Gillet-
- 329 Chaulet, T. Zwinger, A. J. Payne, and a. M. Le Brocq (2014), Retreat of Pine Island
- 330 Glacier controlled by marine ice-sheet instability, *Nat. Clim. Change*, *5*(2), 117–121,
- 331 doi:10.1038/nclimate2094.
- 332 Gagliardini, O., F. Gillet-Chaulet, and M. Montagnat (2009), A review of anisotropic polar
- 333 ice models : from crystal to ice-sheet flow models, in *Physics of Ice Core Records, Vol.*
- 334 *2*, edited by T. Hondoh, Yoshioka, Kyoto, Japan.
- 335 Gillet-Chaulet, F., G. Durand, O. Gagliardini, C. Mosbeux, J. Mouginot, F. Rémy, and
- 336 C. Ritz (2016), Assimilation of surface velocities between 1996 and 2010 to constrain
- 337 the form of the basal friction law under Pine Island Glacier, *Geophys. Res. Lett.*, (1),
- 338 311–321, doi:10.1002/2016GL069937.
- 339 Harland, S. R., J. M. Kendall, G. W. Stuart, G. E. Lloyd, A. F. Baird, A. M. Smith, H. D.
- 340 Pritchard, and A. M. Brisbourne (2013), Deformation in Rutford Ice Stream, West
- 341 Antarctica: measuring shear-wave anisotropy from icequakes, *Ann. Glaciol.*, *54*, 105–
- 342 114, doi:10.3189/2013AoG64A033.
- 343 Hill, R. (1952), The Elastic Behaviour of a Crystalline Aggregate, *Proc. Phys. Soc.*, *65*(5),
- 344 349–354, doi:10.1088/0370-1298/65/5/307.
- 345 Lliboutry, L. (1993), Anisotropic, transversely isotropic nonlinear viscosity of rock ice and
- 346 rheological parameters inferred from homogenization, *Int. J. Plasticity*, *9*, 619–632.
- 347 Ma, Y., O. Gagliardini, C. Ritz, F. Gillet-Chaulet, G. Durand, and M. Montagnat (2010),
- 348 Enhancement factors for grounded ice and ice shelves inferred from an anisotropic ice
- 349 flow model, *J. Glaciol.*, *56*, 805–812, doi:10.3189/002214310794457209.

- 350 Matsuoaka, K., D. Power, S. Fujita, and C. F. Raymond (2012), Rapid development of
351 anisotropic ice-crystal-alignment fabrics inferred from englacial radar polarimetry, cen-
352 tral West Antarctica, *J. Geophys. Res.*, *117*, 1–16, doi:10.1029/2012JF002440.
- 353 Maurel, A., F. Lund, and M. Montagnat (2015), Propagation of elastic waves
354 through textured polycrystals: application to ice, *Proc. R. Soc.*, *471*, 1–28, doi:
355 10.1098/rspa.2014.0988.
- 356 Minchew, B. M., M. Simons, B. Riel, and P. Milillo (2016), Tidally induced variations
357 in vertical and horizontal motion on Rutford Ice Stream, West Antarctica, inferred
358 from remotely sensed observations., *J. Geophys. Res. Earth Surf.*, *122*, 167–190, doi:
359 10.1002/2016JF003971.
- 360 Murray, T., A. M. Smith, M. A. King, and G. P. Weedon (2007), Ice flow modulated by
361 tides at up to annual periods at Rutford Ice Stream, West Antarctica, *Geophys. Res.*
362 *Let.*, *34*, 1–6, doi:10.1029/2007GL031207.
- 363 Nanthikesan, S., and S. Shyam Sunder (1994), Anisotropic elasticity of polycrystalline ice
364 Ih, *Cold Reg. Sci. and Tech.*, *22*(2), 149–169, doi:10.1016/0165-232X(94)90026-4.
- 365 Ng, F. S. L. (2015), Spatial complexity of ice flow across the Antarctic Ice Sheet, *Nat.*
366 *Geosci.*, *8*, 847–852, doi:10.1038/NNGEO2532.
- 367 Picotti, S., A. Vuan, J. M. Carcione, H. J. Horgan, and S. Anandakrishnan (2015),
368 Anisotropy and crystalline fabric of Whillans Ice Stream (West Antarctica) inferred
369 from multicomponent seismic data, *J. Geophys. Res. Solid Earth*, *120*(6), 4237–4262,
370 doi:10.1002/2014JB011591.
- 371 Pimienta, P., P. Duval, and V. Y. Lipenkov (1987), Mechanical behavior of anisotropic
372 polar ice, in *The Physical Basis of Ice Sheet Modelling (Proceedings of the Vancouver*
373 *Symposium)*, pp. 57–66.
- 374 Pollard, D., R. M. DeConto, and R. B. Alley (2015), Potential Antarctic Ice Sheet retreat
375 driven by hydrofracturing and ice cliff failure, *Earth and Planet. Sci. Let.*, *412*, 112–
376 121, doi:10.1016/j.epsl.2014.12.035.
- 377 Savage, M. K. (1999), Seismic anisotropy and mantle deformation: What have we learned
378 from shear wave splitting?, *Rev. Geophys.*, *37*(1), 65–106, doi:10.1029/98RG02075.
- 379 Silver, P. G., and W. W. Chan (1991), Shear wave splitting and subcontinental mantle de-
380 formation, *J. Geophys. Res.*, *96*, 16,429–16,454, doi:10.1029/91JB00899.
- 381 Smith, A. (1997), Basal conditions on Rutford Ice Stream, West Antarctica, from seismic
382 observations, *J. Geophys. Res.*, *102*(B1), 543–552, doi:10.1029/96JB02933.
- 383 Smith, A. M. (2006), Microearthquakes and subglacial conditions, *Geophys. Res. Let.*, *33*,
384 1–5, doi:10.1029/2006GL028207.
- 385 Smith, A. M., and T. Murray (2009), Bedform topography and basal conditions be-
386 neath a fast-flowing West Antarctic ice stream, *Quat. Sci. Rev.*, *28*, 584–596, doi:
387 10.1016/j.quascirev.2008.05.010.
- 388 Smith, E. C., A. M. Smith, R. S. White, A. M. Brisbourne, and H. D. Pritchard (2015),
389 Mapping the ice-bed interface characteristics of Rutford Ice Stream, West Antarc-
390 tica, using microseismicity, *J. Geophys. Res. Earth Surf.*, *120*, 1881–1894, doi:
391 doi:10.1002/2015JF003587.
- 392 Teanby, N. A., J. M. Kendall, and M. Van der Baan (2004), Automation of shear-wave
393 splitting measurements using cluster analysis, *Bull. Seismol. Soc. Am.*, *94*, 453–463, doi:
394 10.1785/0120030123.
- 395 Wuestefeld, A., O. H. Al-Harrasi, J. P. Verdon, J. Wookey, and J.-M. Kendall (2010),
396 A strategy for automated analysis of passive microseismic data to image seis-
397 mic anisotropy and fracture characteristics, *Geophys. Prosp.*, *58*, 755–773, doi:
398 10.1111/j.1365-2478.2010.00891.x.

75 **Figure 1. Earthquake locations on Rutford Ice Stream showing the location of seismic events and**
76 **typical event waveform.** a) Map is in south pole stereographic projection. Purple dots show the location of
77 ~3000 microseismic events generated at the base of the ice stream over a 32-day period. Many events occur
78 in close proximity and overlap in this figure. Location of three-component geophones are red triangles, the
79 orientation of the two horizontal components (X and Y) are shown. Background is Landsat Image Mosaic of
80 Antarctica (LIMA). White arrow shows ice flow direction. b) The waveform of a typical basal microseismic
81 seismic event recorded at a geophone with labelled components. Strong shear waves can be seen on the hori-
82 zontal components and a clear shear wave split can be seen with shear wave ‘S1’ arriving on the cross-stream
83 component (X) before shear wave ‘S2’ arriving later on the down-stream component (Y).

135 **Figure 2. Upper hemisphere plot of splitting measurements.** Splitting measurements (bars) are plotted at
136 their event to station azimuth from north (clockwise around the plot) and ray-path inclination, with the centre
137 of the plot being vertical (0°) and the edge of the plot being horizontal (90°). Measurements are smoothed
138 by taking the average of the measurements in inclination and azimuth bins of $5^\circ \times 5^\circ$. The orientation of each
139 bar represents the polarisation direction of the fast shear wave (Φ) for a given measurement. The length and
140 colour of each bar represents δV_s , percentage S-wave velocity deviation from the isotropic S-wave velocity.
141 The maximum inclination at which good quality measurements were observed was 73° , hence there are no
142 measurements at the outermost edges of the plot.

181 **Figure 3. SWS parameters expected for different ice fabrics.** Left Hand Side: Schematic for each fabric
182 type (adapted from *Maurel et al.* [2015] and *Diez and Eisen* [2015]), with the envelope of c-axes (blue area)
183 and the projection of these c-axes on an upper hemisphere plot (blue dots on the horizontal plane). The angles
184 ξ and θ are used to describe the opening angle of the c-axes envelopes in the X_1 and X_2 directions respec-
185 tively. Right Hand Side: δV_s - the strength of anisotropy (background colour) and direction of the fast shear
186 wave for each fabric type (black bars) on an upper hemisphere plot a) Cluster with an opening angle $\theta = 30^\circ$.
187 b) Thick girdle with opening angle of $\xi = 15^\circ$ c) Vertical partial girdle with an opening angle of $\theta = 15^\circ$. d)
188 Horizontal partial girdle with an opening angle of $\theta = 15^\circ$.

189 **Figure 4. Ice fabric model from shear wave splitting measurements** a) Horizontal partial girdle fabric
190 which makes up 47% of the best fit fabric mixture. Left Hand Side: A schematic of the ice fabric, the envelope of c-axes
191 is within the blue volume, the projection of these c-axes on an upper hemisphere plot is shown (blue dots on the horizontal plane).
192 Right Hand Side: An upper hemisphere plot of modeled shear wave propagation through this fabric, black bars represent the orientation of the fast shear wave and the background
193 colour represents δV_s . Maximum δV_s for this fabric is 9.3%. The orientation of the girdle is near perpendicular to the ice flow direction.
194 b) Broad cluster fabric which makes up 53% of the best fit fabric mixture - the diagram is as in (a). This fabric is weakly anisotropic with a maximum δV_s of 2.1%.
195 c) Best fitting ice fabric model the 'diffuse HPG' - a mixture of 47% horizontal partial girdle and 53% broad cluster. Coloured
196 background and black bars show modeled data. Measured shear wave splitting measurements (coloured bars) are overlain to show fit.
197 Note that the colour scales are different in a, b and c to maximise resolution.
198
199

Figure 1.

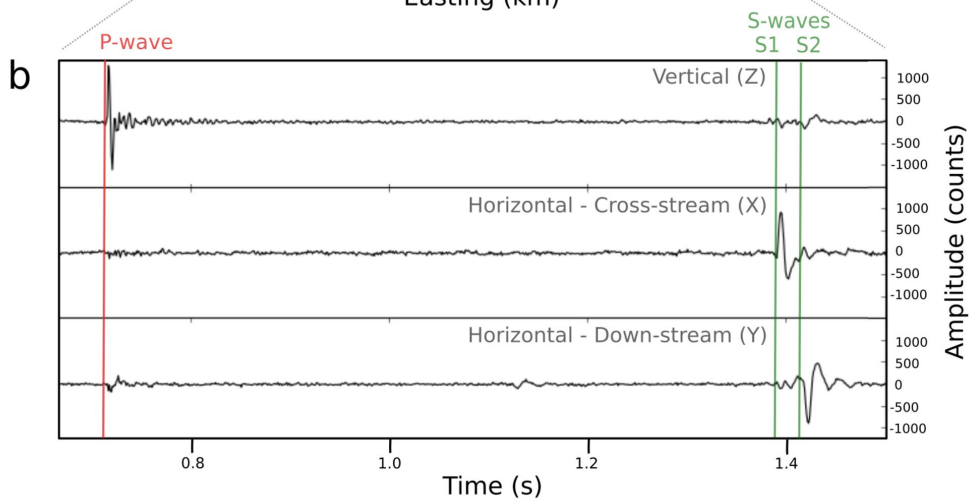
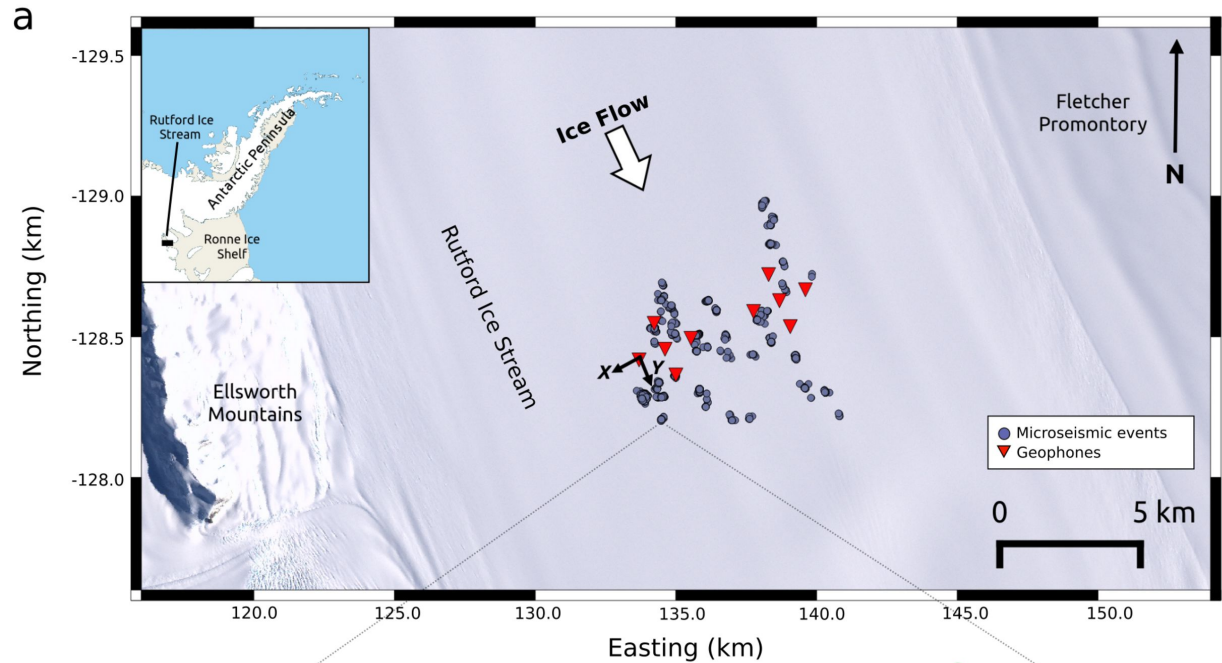


Figure 2.

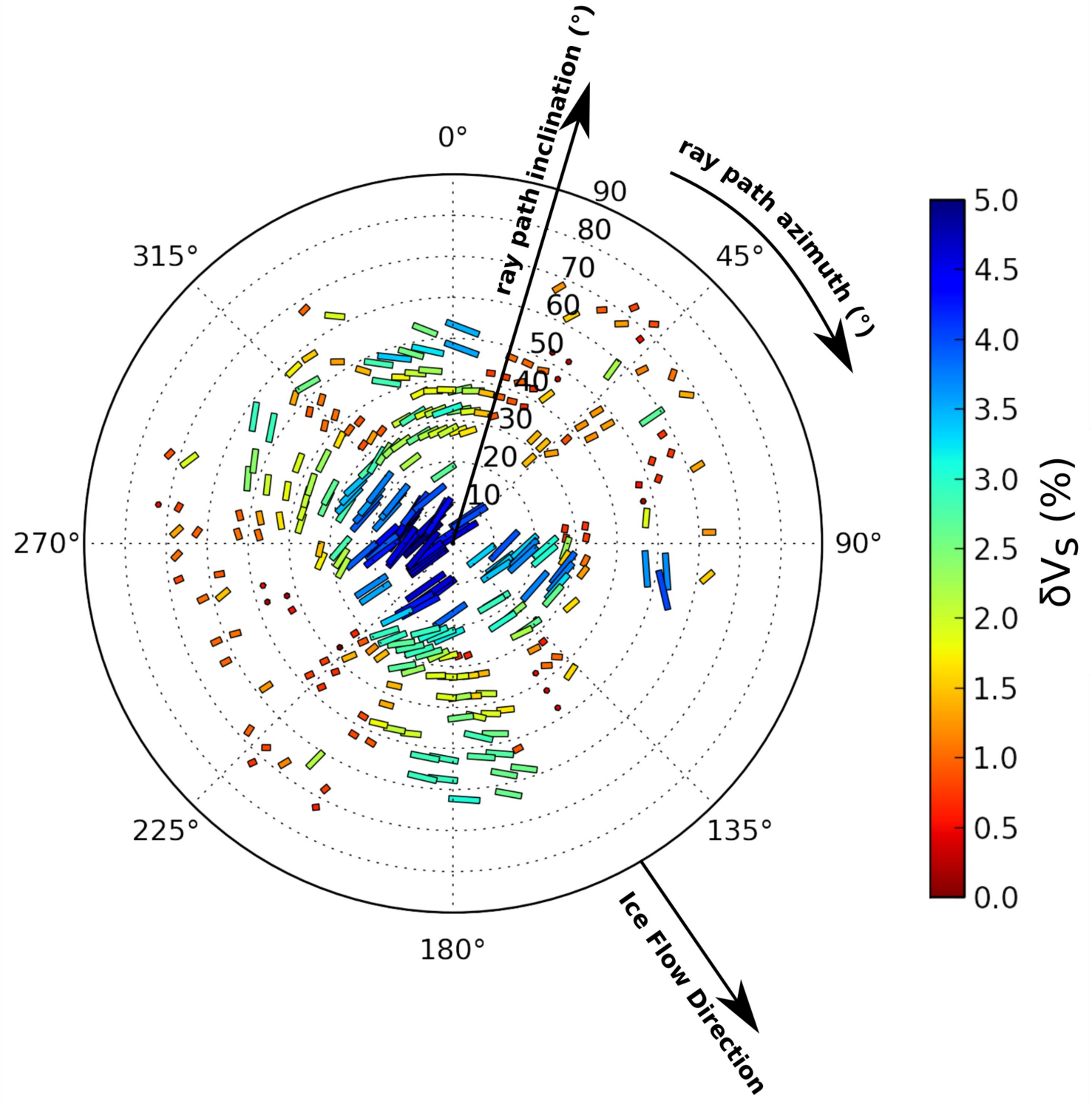
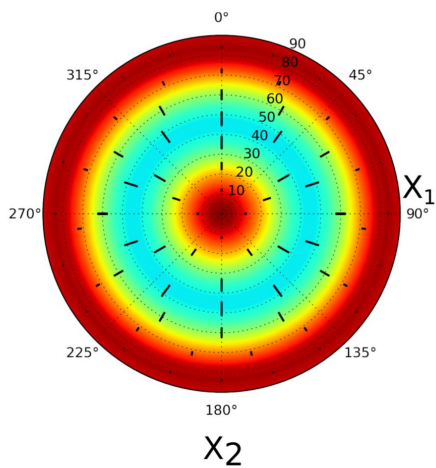
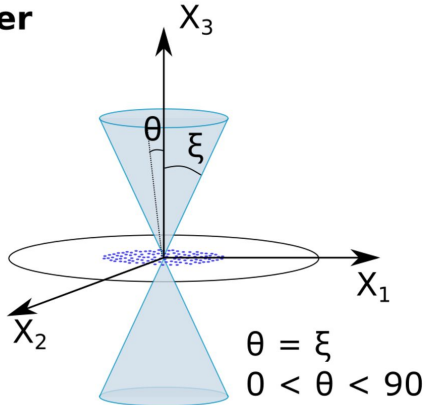
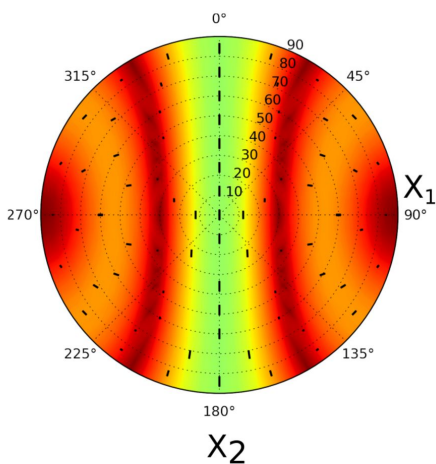
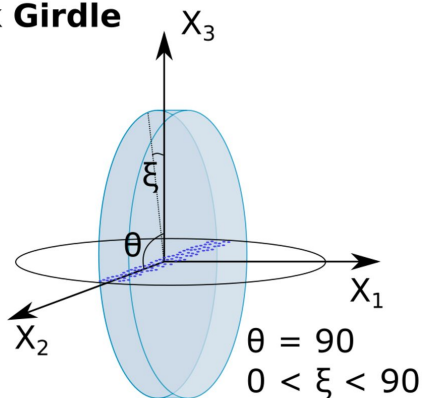


Figure 3.

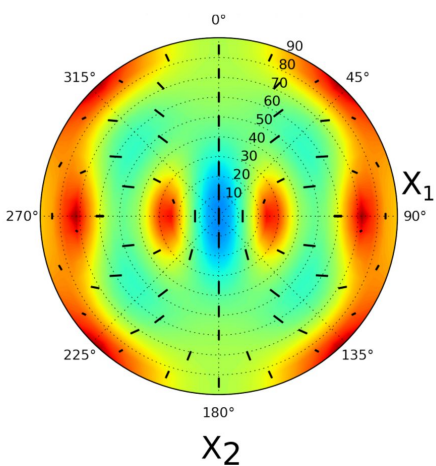
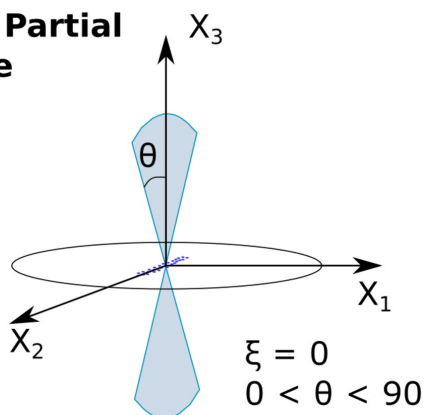
a) Cluster



b) Thick Girdle



c) Vert. Partial Girdle



d) Horiz. Partial Girdle

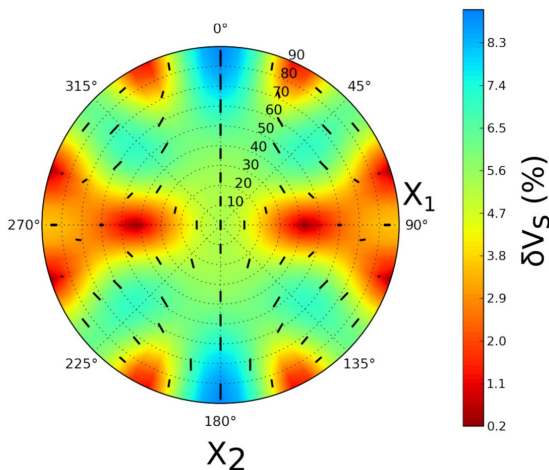
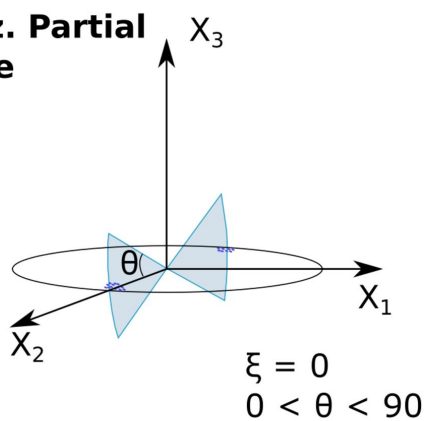
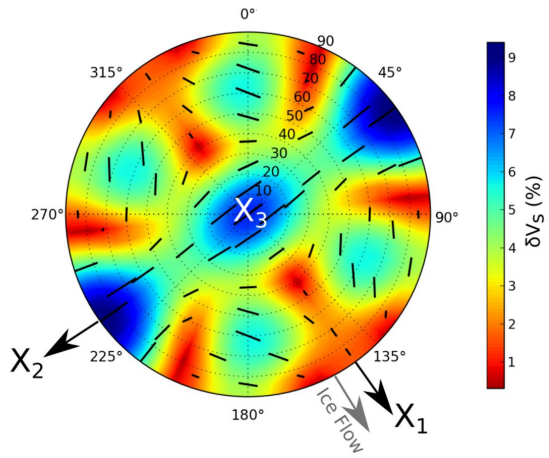
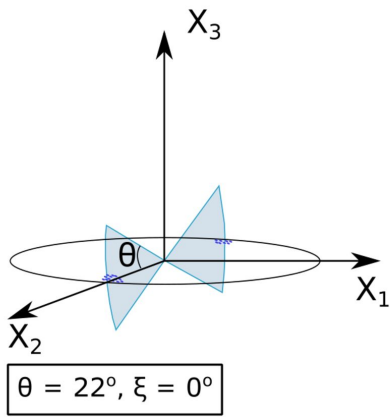
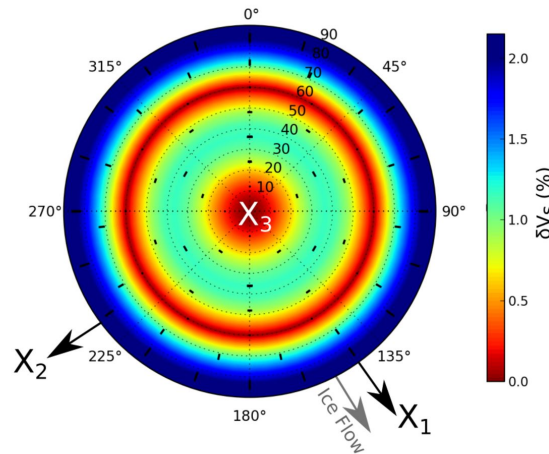
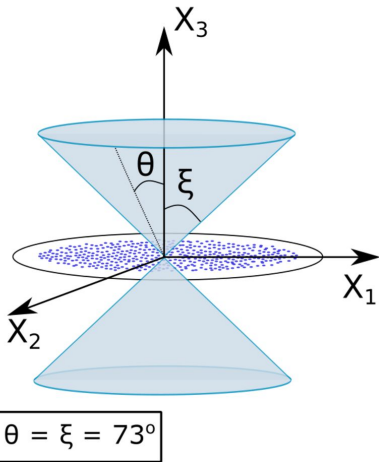


Figure 4.

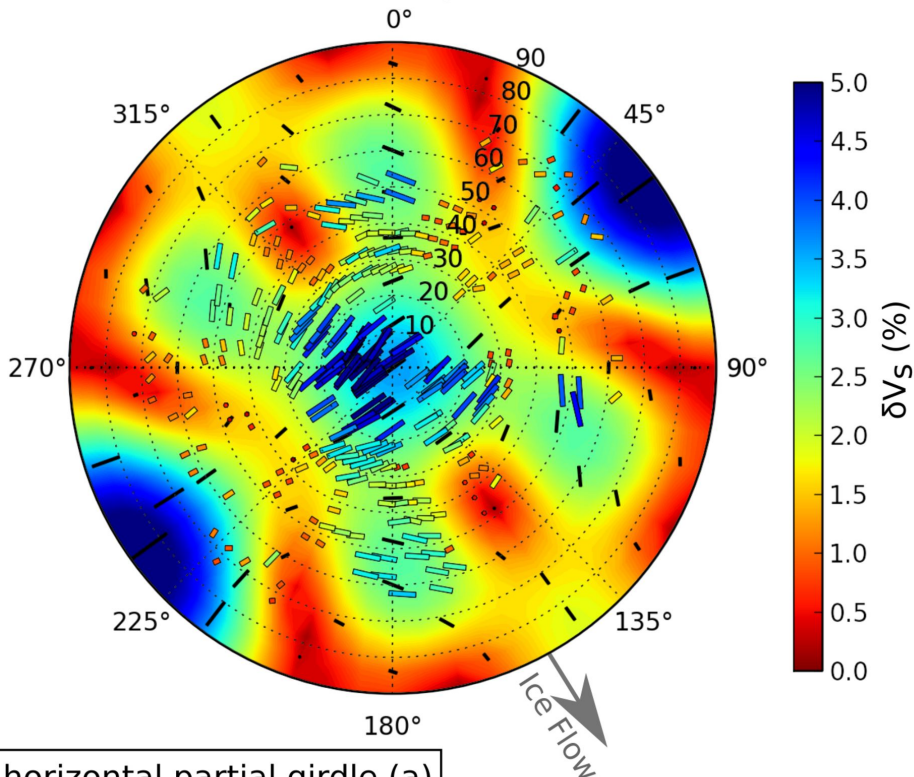
a) Modeled horizontal partial girdle fabric (HPG)



b) Modeled cluster fabric



c) Modeled "Diffuse HPG" fabric (background) with SWS measurements (overlay)



47% horizontal partial girdle (a)
53% cluster (b)